Allosteric Regulation of Substrate Channeling in Tryptophan Synthase: Modulation of the L-Serine Reaction in Stage I of the β-Reaction by α-Site Ligands[†,‡]

Huu Ngo,[§] Novelle Kimmich,[§] Rodney Harris,[§] Dimitri Niks,[§] Lars Blumenstein,[||] Victor Kulik,[||] Thomas Reinier Barends,[||] Ilme Schlichting,[||] and Michael F. Dunn*[,§]

Department of Biochemistry, University of California, Riverside, California 92521, and Department of Biomolecular Mechanisms, Max Planck Institute for Medical Research, Heidelberg, Germany

Received February 25, 2007; Revised Manuscript Received April 17, 2007

ABSTRACT: In the tryptophan synthase bienzyme complex, indole produced by substrate cleavage at the α-site is channeled to the β-site via a 25 Å long tunnel. Within the β-site, indole and L-Ser react with pyridoxal 5′-phosphate in a two-stage reaction to give L-Trp. In stage I, L-Ser forms an external aldimine, E(Aex$_1$), which converts to the α-aminoacrylate aldimine, E(A−A). Formation of E(A−A) at the β-site activates the α-site >30-fold. In stage II, indole reacts with E(A−A) to give L-Trp. The binding of α-site ligands (ASLs) exerts strong allosteric effects on the reaction of substrates at the β-site: the distribution of intermediates formed in stage I is shifted in favor of E(A−A), and the binding of ASLs triggers a conformational change in the β-site to a state with an increased affinity for L-Ser. Here, we compare the behavior of new ASLs as allosteric effectors of stage I with the behavior of the natural product, D-glyceraldehyde 3-phosphate. Rapid kinetics and kinetic isotope effects show these ASLs bind with affinities ranging from micro- to millimolar, and the rate-determining step for conversion of E(Aex$_1$) to E(A−A) is increased by 8−10-fold. To derive a structure-based mechanism for stage I, X-ray structures of both the E(Aex$_1$) and E(A−A) states complexed with the different ASLs were determined and compared with structures of the ASL complexes with the internal aldimine [Ngo, H., Harris, R., Kimmich, N., Casino, P., Niks, D., Blumenstein, L., Barends, T. R., Kulik, V., Weyand, M., Schlichting, I., and Dunn, M. F. (2007) *Biochemistry 46*, 7713−7727].

The allosteric regulation of substrate channeling in the tryptophan synthase bienzyme complex provides an important paradigm for understanding structure−function relationships of molecular processes at the substrate/effector level in metabolic pathways (*1*, *2*). A key component in the allosteric regulation of channeling in the tryptophan synthase system concerns the switching of αβ-dimeric units of the enzyme between open states of low activity and closed states of high activity (Schemes 1−3). In previous work, we proposed that this modulation of conformation and activity synchronizes the catalytic cycles of the α- and β-subunits such that cleavage of IGP[1] at the α-site occurs in phase with formation of the α-aminoacrylate intermediate at the β-site, thereby rendering efficient the conversion of IGP to indole for the synthesis of L-Trp (Schemes 2 and 3) (*1*, *3*−*6*). It has been known for many years that the reaction of L-Ser with the β-subunit activates the α-subunit for cleavage of IGP (*3*, *7*−*9*). Anderson et al. (*8*) proposed and Brzovic et al. (*3*) demonstrated that this activation is triggered by the formation of the α-aminoacrylate intermediate, E(A−A), while Leja et al. (*4*) demonstrated that deactivation of the α-site occurs when the L-Trp quinonoid species, E(Q$_3$), is converted to the L-Trp external aldimine, E(Aex$_2$) (Scheme 2).

Binding studies (*10*, *11*) and kinetic experiments (*3*, *5*, *6*, *8*, *12*−*24*) have shown that the binding of α-site substrates and/or α-site ligands (ASLs) exerts the following effects:

[†] Supported by NIH Grant GM5574 (M.F.D.) and Deutsche Forschungsgemeinschaft (I.S.).

[‡] Structure factors and coordinates have been submitted to the Protein Data Bank as entries 2CLM, 2CLL, 2CLO, and 2J9X.

* To whom correspondence should be addressed: Department of Biochemistry, University of California, Riverside, CA 92521. Phone: (951) 827-4235. Fax: (951) 827-4434. E-mail: michael.dunn@ucr.edu.

[§] University of California.

[||] Max Planck Institute for Medical Research.

[1] Abbreviations: $\alpha_2\beta_2$, native form of tryptophan synthase from *S. typhimurium*; α, α-subunit; β, β-subunit; E(Ain), internal aldimine (Schiff base) intermediate; E(Aex$_1$), external aldimine intermediate formed between the PLP cofactor and L-Ser; E(GD), gem diamine species; E(A−A), α-aminoacrylate Schiff base; E(Q$_1$), L-Ser quinonoid intermediate; E(Q$_3$), quinonoid intermediate that accumulates during the reaction between E(A−A) and indole; E(Aex$_2$), L-Trp external aldimine intermediate; PLS, serine pyridoxal phosphate Schiff base; PLP, pyridoxal phosphate; IGP, 3-indole-D-glycerol 3′-phosphate; IPP, indole-3-propanolphosphate; IAG, indole-3-acetylglycine; GP, α-D,L-glycerol phosphate; G3P, D-glyceraldehyde 3-phosphate; ASL, α-site ligand; F6, *N*-(4′-trifluoromethoxybenzoyl)-2-aminoethyl phosphate; F9, *N*-(4′-trifluoromethoxybenzenesulfonyl)-2-aminoethyl phosphate; F12, *N*-(4′-trifluoromethylphenyl) *N*′-(2-phosphoryloxyethyl)thiourea; F19, *N*-(naphthalene-2′-sulfonyl)-2-aminoethyl phosphate; F21, *N*-(4′-fluorobenzenesulfonyl)-2-aminoethyl phosphate; ANS, 8-anilino-1-naphthalene sulfonate; TEA, triethanolamine; MVC, monovalent cation; $1/\tau_n$, apparent first-order rate constant of the *n*th relaxation; A_n, amplitude of the *n*th relaxation; K_{Dapp}, apparent dissociation constant; $1/\tau_n^{ASL}$, apparent first-order rate constants measured for enzyme species with bound ASLs; KIE, kinetic isotope effect. Structural elements of tryptophan synthase are designated as follows: loop αL2, residues α53−60; loop αL6, residues α179−193; helix αH8, residues α249−265; COMM domain, residues β102−189; helix βH5, residues β145−150; helix βH6, residues β165−181.

10.1021/bi7003872 CCC: $37.00
Published on Web 06/09/2007

Scheme 1: (A) Organic Chemistry of the α- and β-Reactions and (B) Comparison of the Structures of α-Site Substrates with the α-Site Ligands Used in This Study

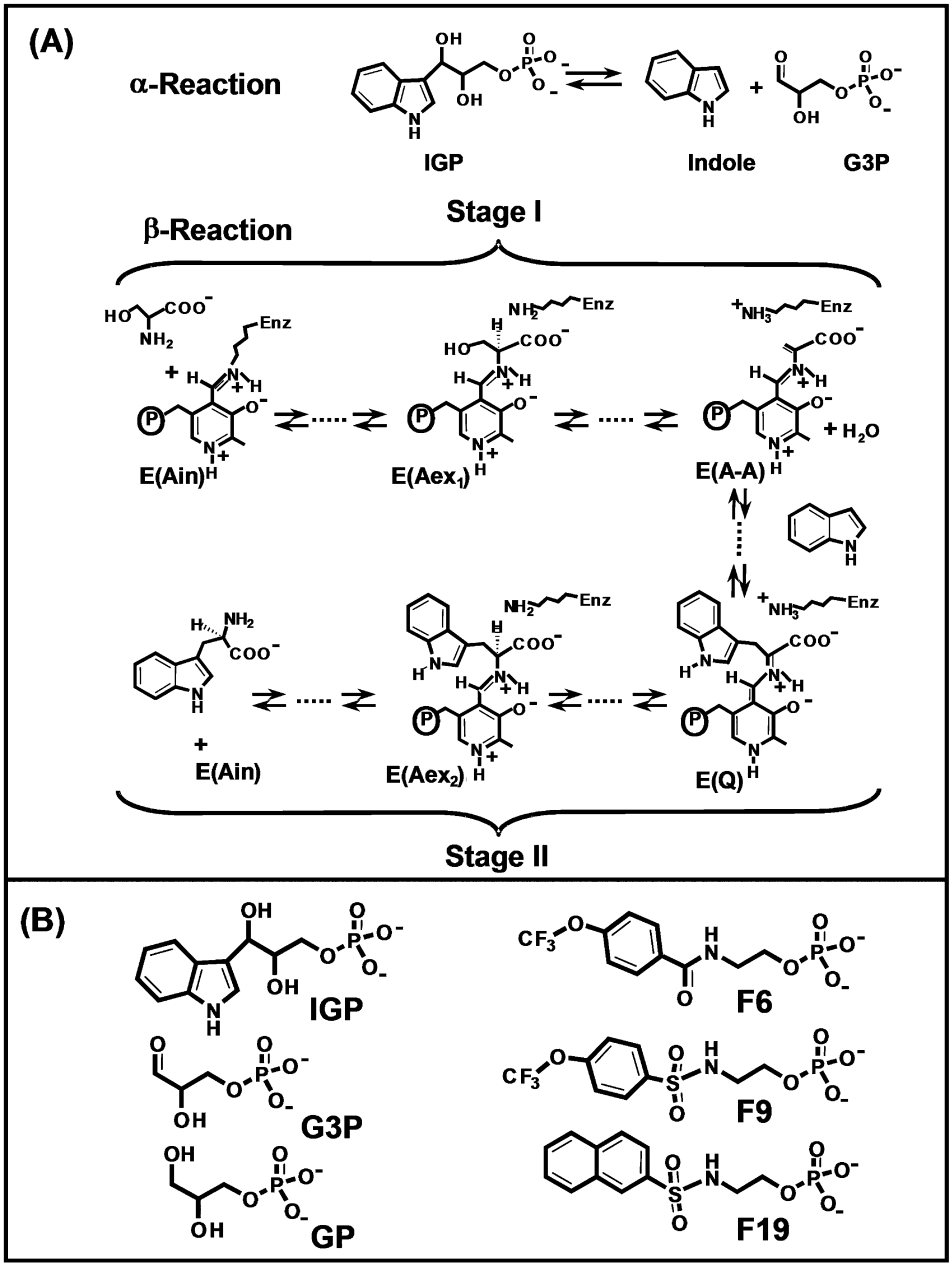

(a) a strong perturbation of the binding of substrate and substrate analogues to the β-site of E(Ain), (b) alteration of the distribution of intermediates formed in stage I of the β-reaction [the reaction of L-Ser with the internal aldimine, E(Ain)] (Scheme 1A), and (c) perturbation of the kinetics of the β-reaction. However, the implications of these interactions for the regulation of catalysis and/or channeling remain an open question. In this work, we employ solution kinetic studies of complexes formed with D-glyceraldehyde 3-phosphate (G3P), D,L-glycerol 3-phosphate (GP), and four new IGP analogues, F6, F9, F12, and F19 (Scheme 1B) (*23*), and we have determined the structures of four of these complexes by X-ray diffraction as part of a detailed investigation into the roles played by the binding of ASLs during stage I of the β-reaction. This work includes the first reported structure of the native enzyme, in the form of the (GP)E(A−A) complex, with both the α- and β-subunits in the closed conformations. It will be shown that ASL binding can significantly accelerate the rate-determining step for stage I of the β-reaction. The implications of this activation for the regulation of substrate channeling are discussed.

MATERIALS AND METHODS

Materials. L-Ser, the diethylacetal of D-glyceraldehyde 3-phosphate (G3P), and D,L-glycerol 3-phosphate (GP) were purchased from Sigma as the highest-purity materials available and used without further purification. The diethylacetal of G3P was converted to G3P according to the manufacturer's instructions. The procedures for the synthesis and purification of F6, F9, F12, and F19 are described elsewhere (*23*). The samples of [α-^{2}H]-L-Ser used in the measurement of kinetic isotope effects were prepared as previously described (*5*). Purification of wild-type tryptophan synthase from *Salmonella typhimurium* was performed as previously described (*5*, *25*−*27*). All solution studies were carried out in the presence of 100 mM NaCl to keep the enzyme in the

Scheme 2: Dependence of the Activity of the α-Site on the Covalent State of the β-Subunit[a]

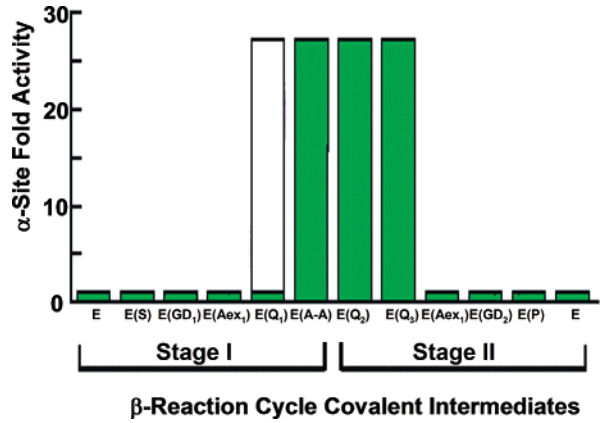

[a] Redrawn from ref *1*.

Scheme 3: Cartoon Depicting Conformational Equilibria for the Switching between Open and Closed States[2] of the αβ Dimeric Unit

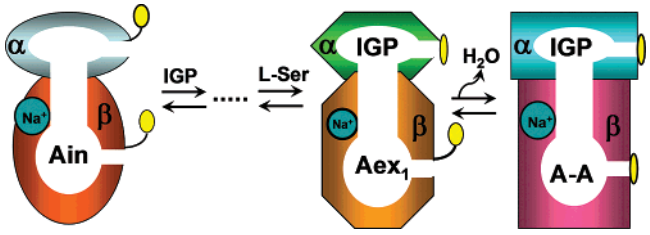

Na^+-activated form (*28*), and unless otherwise stated, all of the reactions were conducted at 25 °C in 50 mM TEA buffer (pH 7.8).

Static and Stopped-Flow Kinetic UV−Vis Absorbance and Fluorescence Measurements. Absorbance and fluorescence spectra, stopped-flow kinetic measurements, and activity measurements were performed as previously described (*5*, *6*). Kinetic time courses were fitted by nonlinear least-squares regression analysis using Peakfit (version 4, Jandel Scientific) to a sum of exponentials according to eq 1

$$Ø = Ø_\infty \pm \sum_i Ø_i \exp(t/\tau_i) \quad (1)$$

where $Ø_t$ is the absorbance or fluorescence at time t, $Ø_\infty$ is the final value of the absorbance or fluorescence, $Ø_i$ is the absorbance or fluorescence due to the ith relaxation, and $1/\tau_i$ corresponds to the observed rate for the ith relaxation.

Crystallization, Complex Formation, Diffraction Data Collection, and Refinement. Tryptophan synthase was purified and crystallized as previously described (*29*). Complex formation was achieved by soaking native crystals for 10 min in a solution containing 90 mM Bis-Tris-Propane (pH 7.8), 150 mM NaCl, 15% (w/v) PEG 8000, 20% glycerol, 200 mM Na^+-L-Ser, and 10 mM F6, F9, or F19. For the formation of the E(A−A) complex, crystals were soaked in 100 mM MES (pH 6.5), 200 mM CsCl, 15% (w/v) PEG 8000, 20% glycerol, 200 mM Na^+-L-Ser, 100 mM GP, and 100 mM indole dissolved in DMSO. Diffraction data were collected at the European Synchrotron Radiation Facility (ESRF, Grenoble, France) or the Swiss Light Source (SLS, Paul-Scherrer Institute, Villingen, Switzerland) with the crystals kept at 100 K (Table 1). The data were processed with XDS (*30*). The indole-3-propanolphosphate (IPP) complex with E(Ain) (PDB entry 1QOP) was used as a starting model for structure determination. To reduce model bias, the coordinates of loops αL2 and αL6, IPP, PLP, the sodium ion, and all water molecules were omitted. For each structure, the initial model was divided into three parts [α-subunit, COMM domain (*29*), and the core of the β-subunit] that were subjected to rigid body and simulated annealing refinement via CNS 1.0 or 1.1 (*31*). Clear electron density was observed for F6, F9, F19, and the serine pyridoxal phosphate Schiff base (PLS) as well as for GP and the α-aminoacrylate after the first cycle of simulated annealing refinement. Thus, these parts of the structure were included in the subsequent refinement steps. The same was true for loops αL2 and αL6 in the (F9/F19)E(Aex_1) and (GP)E(A−A) complexes. In contrast to these structures, poor density was observed in the F6 complex for αL6, and this loop was therefore not included in the refinement. In the case of the (GP)E(A−A) complex, there was electron density for three DMSO molecules that reside at solvent-exposed regions that are most likely irrelevant to the enzymatic function. Although the soaking solution contained indole, an attempt to generate a quinonoid complex, there was no electron density accounting for an indole moiety. Most water molecules were placed automatically using the CNS Waterpick routine. Structures were superimposed with O (*32*) and Xfit (*33*) using all C_α atoms for each pair of structures except for those belonging to loop αL2, loop αL6, and the COMM domain.

RESULTS

Characterization of the Effects of α-Site Ligands on the Equilibrium Distribution of Intermediates in the Reaction of L-Ser with Tryptophan Synthase. Stage I of the β-reaction has been the subject of extensive investigation via equilibrium measurements, rapid mixing stopped-flow studies, and pressure jump relaxation (*5*, *8*, *16*, *28*, *34*−*38*). At pH 7.8 and 25 °C, the reaction of L-Ser with the $\alpha_2\beta_2$ form of tryptophan synthase (stage I of the β-reaction) gives an equilibrium distribution of species dominated by comparable amounts of the external aldimine intermediate (λ_{max} = 425 nm) and the α-aminoacrylate intermediate (λ_{max} = 350 and 460 nm) (Figure 1) (*35*, *37*, *39*). The distribution of these intermediates is influenced by pH, temperature, pressure, monovalent cation binding, and ASL binding (*10*, *11*, *22*, *23*, *28*, *36*, *38*, *40*−*42*). In these kinetic studies, the Na^+-activated form of the enzyme is used throughout. It is well-established that the binding of structural analogues of IGP and/or G3P causes a redistribution of the intermediates formed in stage I of the β-reaction in favor of E(A−A) (*5*, *6*, *8*, *10*, *11*, *13*, *16*, *23*, *28*, *36*, *43*). The UV−vis absorption spectra presented in Figure 1 show that the ASLs used in this study are effective in mediating this redistribution. These α-site ligands cause an increase in the intensities of the spectral bands at 350 and 460 nm assigned to the E(A−A) intermediate and a diminution of the intensity of the 425 nm band of the E(Aex_1) intermediate. Of the ASLs that were examined, F9 is the most effective in driving this redistribution.

Influence of ASLs and Substitution of ^2H for ^1H at the C_α of L-Ser on the Kinetics of E(Aex_1) Formation and Decay. In the absence of an ASL, the kinetics of stage I (see Scheme

Table 1: Crystal Parameters, Data Collection, and Refinement Statistics

	(F6)E(Aex$_1$)	(F9)E(Aex$_1$)	(F19)E(Aex$_1$)	(GP)E(A−A)
PDB entry	2CLM	2CLL	2CLO	2J9X
crystal parameters				
space group	*C*2	*C*2	*C*2	*C*2
unit cell dimensions				
a, *b*, *c* (Å)	182.5, 59.4, 67.7	182.5, 59.8, 67.3	182.7, 60.1, 67.5	183.2, 60.8, 67.4
β (deg)	94.84	94.61	94.66	94.63
data collection				
beamline	14-4	14-1	X10SA	14-1
X-ray source	ESRF	ESRF	SLS	ESRF
wavelength (Å)	1.040	0.931	0.905	0.934
data statistics				
resolution (Å)	20−1.5	19.4−1.5	20−1.45	20−1.7
no. of observations	293946	229734	163	195251
no. of unique reflections	102736	116340	124324	74159
completeness (total/high) (%)[a]	88.6/49.6	81.8/90.2	96.1/94.5	91.0/95.5
⟨*I*/*σ*(*I*)⟩ (total/high)[a]	12.4/2.4	17.3/3.7	6.5/1.7	10.1/2.0
R_{sym} (total/high)[a,b]	5.4/35.1	4.3/38.9	13.8/63.1	8.5/49.3
refinement statistics				
resolution range (Å)	20−1.5	20−1.6	10−1.5	20−1.9
refinement program	CNS 1.1	CNS 1.0	CNS 1.1	CNS 1.1
included amino acids	A 1−178	A 1−184	A 1−184	A 1−189
	A 194−267	A 194−267	A 194−268	A 193−267
	B 2−393	B 2−394	B 2−391	B 2−395
no. of protein atoms	4874	4855	4899	4881
no. of waters	642	522	568	418
no. of ligand atoms	43	44	43	43
no. of Na^+ ions	1	1	1	-
no. of Cs^+ ions	−	−	−	3
R_{work} (%)/R_{free} (%)[c]	21.8/23.9	21.7/24.5	23.2/24.9	21.5/24.0
rms deviation for bonds (Å)	0.006	0.015	0.006	0.0011
rms deviation for angles (deg)	1.29	1.62	1.27	1.54

[a] Completeness, R_{sym}, and ⟨*I*/*σ*(*I*)⟩ are given for all data and for the highest-resolution shell. Resolution shells are as follows: 1.5−1.6 Å (F6), 1.6−1.7 Å (F9), 1.55−1.65 Å (F9), and 2.0−1.9 Å (GP). [b] $R_{sym} = \sum|I - \langle I\rangle|/\sum I$. [c] $R_{work} = \sum|F_{obs}| - k|F_{calc}|/\sum|F_{obs}|$. Five percent of randomly chosen reflections were used for the calculation of R_{free}.

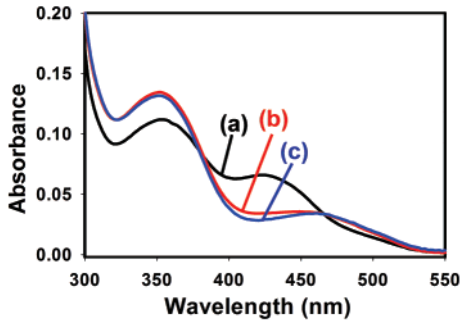

FIGURE 1: Static UV−vis spectra showing the influence of α-site ligands on the absorption spectrum of tryptophan synthase following reaction with 40 mM L-Ser in stage I of the *β*-reaction (Scheme 1): (a) no ASL, (b) 4 mM G3P, and (c) 200 *μ*M F9. The absorption bands for the PLP intermediates have been previously identified as the internal aldimine species (λ_{max} = 412 nm), the external aldimine species (λ_{max} = 425 nm), and the α-aminoacrylate species (λ_{max} = 350 nm). The λ_{max} ∼ 460 nm shoulder is also due to the α-aminoacrylate species (*35*, *39*, *59*).

1) consist of a rapid process in which E(Aex$_1$) transiently accumulates and then decays to an equilibrium mixture dominated by E(Aex$_1$) and E(A−A) (*34*, *35*). The Michaelis complex, E(Ain)(L-Ser), is formed within the mixing dead time of the stopped-flow apparatus, and there is no significant buildup of the L-Ser gem diamine species, E(GD$_1$). The L-Ser quinonoid intermediate, E(Q$_1$), can be detected as a transient species; however, the amount that accumulates is very small (*35*). The appearance and decay of E(Aex$_1$) are conveniently observed using rapid mixing methods by exploitation of the strong fluorescence emission of this species (λ_{ex} = 425 nm, and λ_{em} ∼ 500 nm) (*34*, *35*). Other intermediates along the reaction path exhibit very little fluorescence arising from excitation at 425 nm (*34*). The time course for formation of E(Aex$_1$) in the absence of an ASL (Figure 2A,D, trace a) is dominated by a single exponential (the phase of increasing fluorescence emission, τ_1). The decay process (of decreasing fluorescence) to give the E(A−A) species is more complicated and consists of a dominating relaxation (τ_2) followed by two slower relaxations (τ_3 and τ_4), each with relatively small amplitudes and slow rates (*5*, *34*, *35*). Relaxations τ_3 and τ_4 have been proposed to represent processes that result in small readjustments of the distribution of E(Aex$_1$) and E(A−A) (*35*) and to the interconversion of inactive and active forms of E(A−A) (*34*, *35*, *38*) and were not investigated further in this work.

In good agreement with earlier work using GP as an IGP or G3P analogue (*3*, *13*−*15*), inspection of the time courses in panels A and D of Figure 2 shows that the relaxation rates both for the formation ($1/\tau_1^{ASL}$) and for the decay ($1/\tau_2^{ASL}$) of E(Aex$_1$) are significantly affected by the binding of ASLs. For each of the ASLs that were studied, ASL binding decreases $1/\tau_1$ and increases $1/\tau_2$. These time courses can be fitted well to the general kinetic expression given in eq 1. Depending on the time scale observed and the concentration of L-Ser used, as many as four exponentials are needed to fit the data, where E(Aex$_1$) is formed in the first relaxation ($1/\tau_1^{ASL}$) and decays to an equilibrium distribution of E(Aex$_1$)

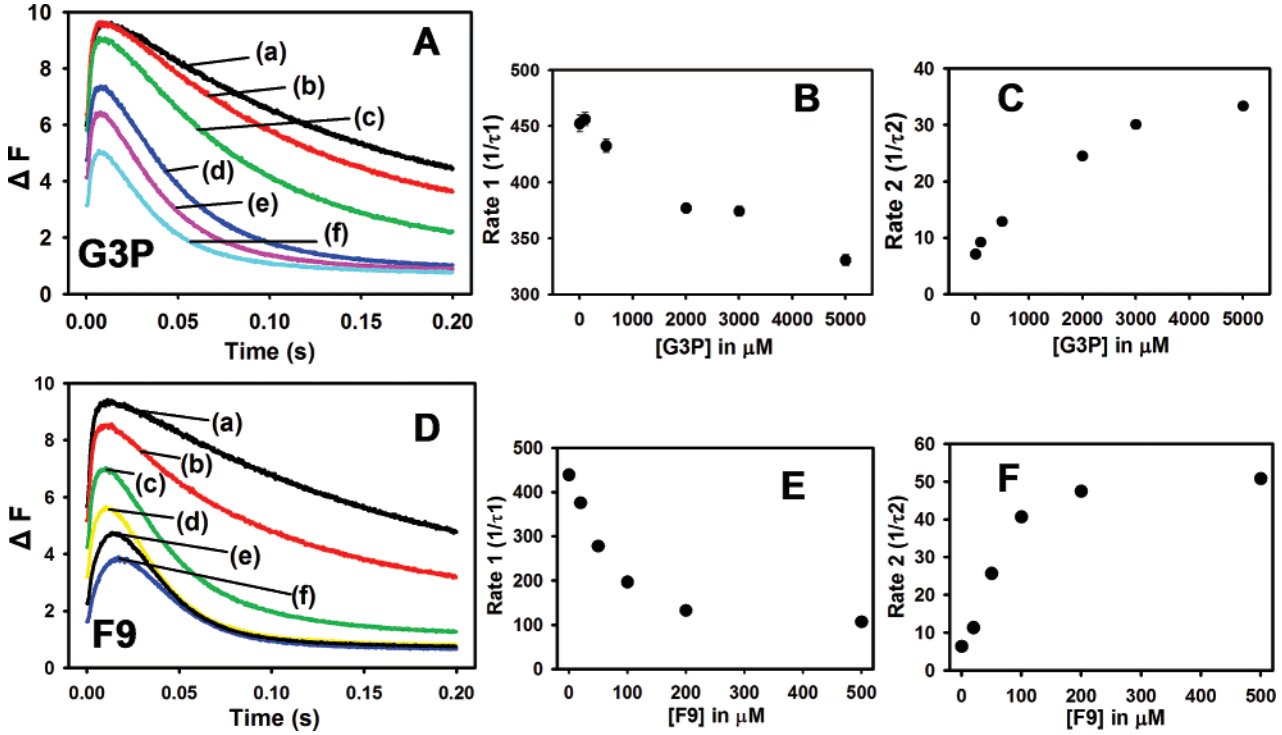

FIGURE 2: Effects of ASLs on the stopped-flow fluorescence time course for the formation and decay of the E(Aex$_1$) intermediate in stage I of the β-reaction. Panels A and D show typical fluorescence time courses comparing the reaction of 8 mM L-Ser in the absence (trace a) of any ASL and in the presence of either G3P (A) or F9 (D): (A) 100, 500, 2000, 3000, and 5000 μM G3P for traces b−f, respectively, and (D) 20, 50, 100, 200, and 500 μM F9 for traces b−f, respectively. Panels B, C, E, and F compare the dependencies of the relaxation rates for the appearance, $1/\tau_1$, and decay, $1/\tau_2$, of the external aldimine species on ASL concentration: G3P for panels B and C and F9 for panels E and F.

Table 2: Summary of Relaxation Rates, Kinetic Isotope Effects, and ASL Activation Ratios Obtained from Analysis of the Fluorescence Time Courses for the Reaction of L-Ser with E(Ain) in the Presence of an ASL[a]

ASL	^{1}H $1/\tau_1$ (s^{-1}) (8 mM L-Ser)	^{1}H $1/\tau_2$ (s^{-1}) (50 mM L-Ser)	^{2}H $1/\tau_2$ (s^{-1}) (50 mM L-Ser)	(α-^{1}H $1/\tau_2$)/(α-^{2}H $1/\tau_2$) KIE	ASL activation[b] α-^{1}H L-Ser	ASL activation[b] α-^{2}H L-Ser
no ASL	430	5.7	2.0	2.9	0.0	0.0
500 μM F6	340	50	12.5	4.0	8.8	6.3
500 μM F9	110	55	9.8	5.6	9.7	4.9
500 μM F12	350	40	10.0	4.0	6.9	5.0
500 μM F19	86	26	9.6	2.7	4.6	4.8
17 mM G3P	330[c]	41	16.0	2.6	7.2	8.0
100 mM GP	140[d]	47	11.7	4.0	8.2	5.9

[a] Time courses were measured by monitoring the fluorescence emission from the E(Aex$_1$) intermediate (see Figures 2 and 3). Experimental errors typically were less than ±10% for the reported rate constants; KIEs were less than ±15%, and the activation ratios were less than ±15%. [b] Activation ratios were calculated as the ratio of the rate measured in the absence of an ASL divided by the rate measured in the presence of the ASL. [c] Reaction with 5 mM G3P. [d] Reaction with 50 mM GP.

and E(A−A) in the three subsequent relaxations (τ_2^{ASL}, τ_3^{ASL}, and τ_4^{ASL}) (eq 2).

$$F_t = \Delta F_1^{ASL} \exp(-t/\tau_1^{ASL}) - \Delta F_2^{ASL} \exp(-t/\tau_2^{ASL}) - \Delta F_3^{ASL} \exp(-t/\tau_3^{ASL}) - \Delta F_4^{ASL} \exp(-t/\tau_4^{ASL}) + F_0 \quad (2)$$

In eq 2, F_t is the fluorescence intensity at time t, ΔF_1^{ASL}, ΔF_2^{ASL}, ΔF_3^{ASL}, and ΔF_4^{ASL} are the amplitudes of the phases corresponding to the formation and decay of E(Aex$_1$), and $1/\tau_1^{ASL}$, $1/\tau_2^{ASL}$, $1/\tau_2^{ASL}$, and $1/\tau_2^{ASL}$ are the relaxation rates of these phases. ΔF_0 is the fluorescence at time zero. For each ASL, the relaxation rate, $1/\tau_1^{ASL}$, is sensitive to the concentration of L-Ser up to concentrations of >10 mM. Depending on the particular ASL, at high L-Ser concentrations (>10 mM), $1/\tau_1^{ASL}$ may become too large to be accurately determined by stopped-flow methods due to the loss of amplitude in the mixing dead time (~2 ms in this study). Consequently, at 50 mM L-Ser, most of the fluorescence change in τ_1^{ASL} is lost in the mixing dead time, and the time courses are dominated by the decay of E(Aex$_1$) to E(A−A) in τ_2^{ASL}. Since the rates and amplitudes of $1/\tau_3^{ASL}$ and $1/\tau_4^{ASL}$ are small and irrelevant to the objectives of this study, no analysis of these relaxations is presented here.

Panels B and E of Figure 2 show typical dependencies of $1/\tau_1^{ASL}$ on ASL concentration for G3P and F9 measured at an L-Ser concentration of 8.0 mM, conditions under which $1/\tau_1^{ASL}$ can be measured with reasonable accuracy and precision. These data establish that $1/\tau_1^{ASL}$ decreases and then tends toward a saturating value as the concentration of the ASL is increased. Table 2 compares $1/\tau_1$ with the values of $1/\tau_1^{ASL}$ measured at 8.0 mM L-Ser and 500 μM ASL, conditions under which the $1/\tau_1^{ASL}$ values are nearly inde-

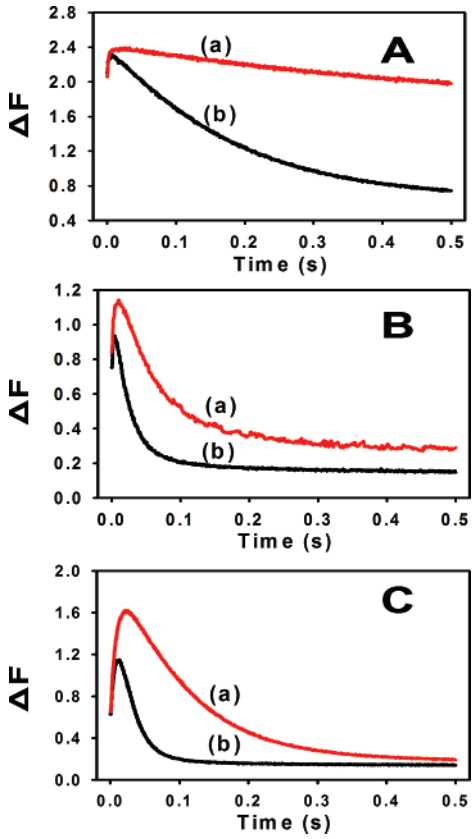

FIGURE 3: Comparisons showing the effects of ASLs and the substitution of ^{2}H (trace a) for ^{1}H (trace b) at the C-α of L-Ser on typical stopped-flow fluorescence time courses for the decay of the E(Aex$_1$) intermediate: (A) no ASLs, (B) 17 mM G3P, and (C) 500 μM F9.

pendent of ASL concentration. The decrease in $1/\tau_1^{ASL}$ depends on the structure of the ASL. The data presented in panels C and F of Figure 2 show that $1/\tau_2^{ASL}$ values increase with increasing ASL concentration and then approach saturating values at high concentrations.

The kinetic traces in Figure 3 compare both the effects of ASLs on $1/\tau_2^{ASL}$ and the substitution of ^{2}H for ^{1}H at the C$_\alpha$ of L-Ser on the primary KIE measured at high (50 mM) L-Ser (where $1/\tau_1^{ASL} > 1/\tau_2^{ASL}$). Analysis of $1/\tau_2^{ASL}$ (Figure 3A−C and Table 2) shows that, depending on the ASL, the rate of decay of E(Aex$_1$) to E(A−A) is increased 6−10-fold by ASL binding. When the concentration dependencies of the decay rates are extrapolated to high ASL concentrations, the predicted decay rates approach similar, saturated values. The effectiveness of a given ASL (F9 > F19 > F6 ∼ F12 ∼ GP > G3P) appears to be related to the apparent affinity of the ASL for the α-site. Table 2 shows that there is a large apparent kinetic isotope effect ($k^H/k^D = 2.6-5.6$) on $1/\tau_2^{ASL}$ when [α-^{2}H]-L-Ser is substituted for [α-^{1}H]-L-Ser. The magnitudes of the apparent isotope effects are different for the different ASLs (ranging from 2.6 for G3P to 5.6 for F9).

Influence of ASLs on the Kinetics of E(A−A) Formation. Panels A and B of Figure 4 present typical absorbance time courses measured at 350 nm comparing the effects of G3P, F6, F9, F12, and F19 on stage I of the β-reaction with the reaction in the absence of an ASL with either [α-^{1}H]-L-Ser (Figure 4A) or [α-^{2}H]-L-Ser (Figure 4B). These time courses are characterized by a brief initial phase (50−100 ms duration) during which the absorbance at 350 nm very

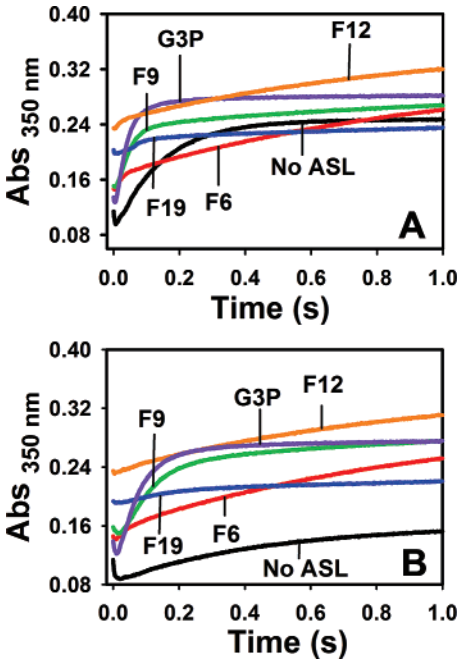

FIGURE 4: Typical single-wavelength stopped-flow absorbance time courses measured at 350 nm for the reactions of isotopically normal (A) and α-^{2}H-substituted L-Ser (B) in stage I of the β-reaction. The time course compare the effects of 5 mM G3P, 50 mM GP, 10 mM F6, 10 mM F9, 10 mM F12, and 10 mM F19 on stage I of the β-reaction with the reaction in the absence of an ASL. Experimenal conditions: [αβ] = 40 μM, [L-Ser] = 8 mM, [[α-^{2}H]-L-Ser] = 8 mM, and [NaCl] = 100 mM.

slightly decreases. This phase corresponds to the relaxation associated with formation of E(Aex$_1$) detected in the fluorescence experiments (i.e., τ_1^{ASL}) (Figure 2). Following this relaxation, a slower phase (τ_2^{ASL}) occurs in which the 350 nm band of the E(A−A) intermediate appears. This phase is fitted well by truncating the time course to remove the initial relaxation (the first ∼100 ms) and then analyzing the remaining time course (at times of >100 ms) as a single exponential with a rate $1/\tau_2^{ASL}$ (eq 3).

$$A_t = \Delta A_2^{ASL} \exp(-t/\tau_2^{ASL}) + A_0 \quad (3)$$

In eq 3, A_t is the absorbance at any time, t, A_2^{ASL} is the amplitude of the relaxation, $1/\tau_2^{ASL}$, and A_0 is the absorbance at time zero. The values of $1/\tau_2^{ASL}$ measured by the absorbance change at 350 nm (data not shown) give good agreement with the values measured for $1/\tau_2^{ASL}$ in the fluorescence experiments (Figures 2 and 3) and show the same isotope effects.

Crystal Structures of E(Aex$_1$) Complexes in the Presence of Different ASLs. In previous studies, we have shown how the binding of different ligands at the α-site modulates the conformation of the β-site through intersubunit communication in the internal aldimine state, E(Ain) (*23*). Figure 5A−C compares the structures of the (ASL)E(Aex$_1$) complexes of F9 (A), F19 (B), and F6 (C) with the respective (ASL)E(Ain) complexes [PDB entries 2CLE (F6 at a low concentration), 2CLF (F6 at a high concentration), 2CLI (F9), and 2CLH (F19)]. These ASLs all bind to the α-site of E(Aex$_1$) in the same way as in the corresponding (ASL)E(Ain) complexes. The phosphoryl group of each ASL is located at the same position and forms the usual contacts with helix αH8′ (*23*, *44*), while the hydrophobic naphthyl or phenyl

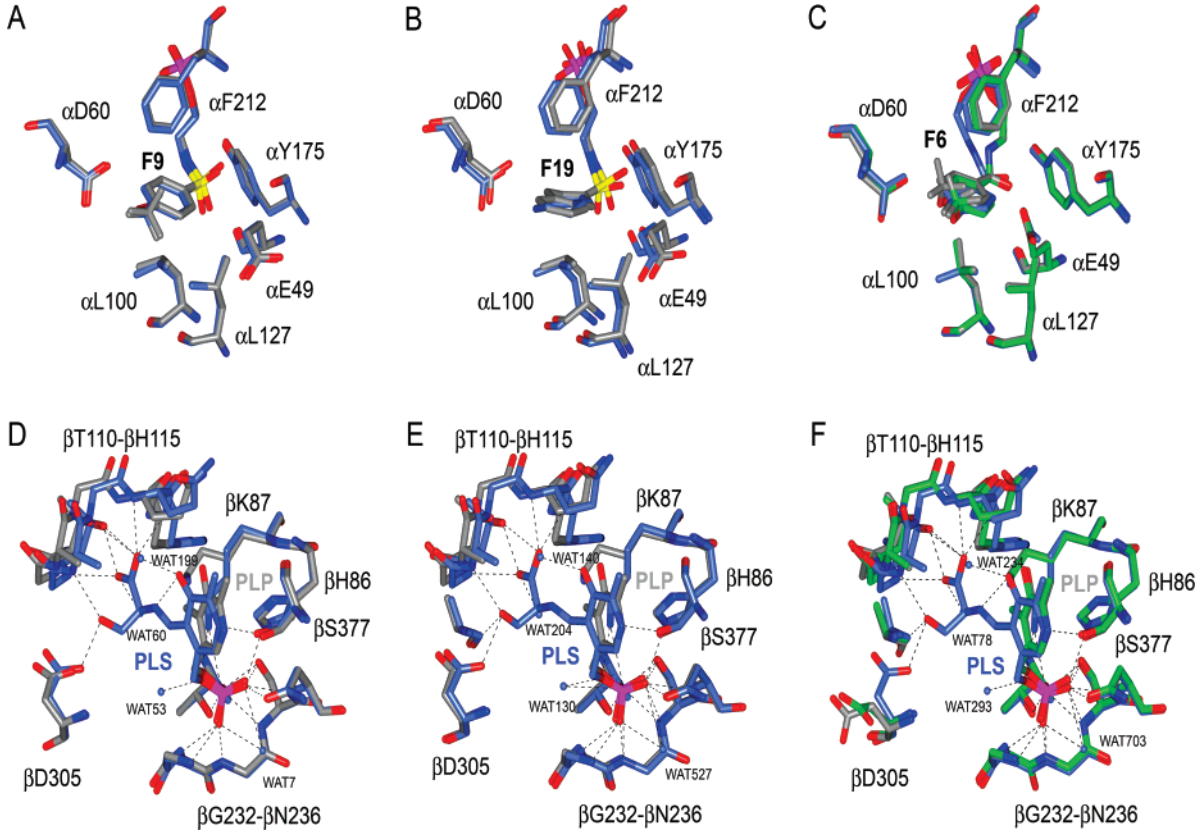

FIGURE 5: Overlay of the E(Ain) and E(Aex$_1$) states at the α- and β-sites in the presence of different ASLs. (A−C) Comparison of the α-site of the E(Ain) (gray) and E(Aex$_1$) (light blue) states in complex with F9 (A), F19 (B), and F6 (C). (D−F) Details of the binding of PLS in the β-site. For comparison, the E(Aex$_1$) states complexed with F9 (D), F19 (E), and F6 (F) (depicted in light blue) were superimposed with the respective E(Ain) complexes (gray). For all F6 complexes, the E(Ain)(high-F6) complex (green, PDB entry 2CLF) was overlaid in addition to the other two complexes.

rings are sandwiched between the side chains of αF212, αL100, and αL127. The terminal trifluoromethyl groups of the F6 and F9 complexes occupy a hydrophobic pocket made up by the side chains of αI153, αL175, αA129, and βP18 at the subunit interface in the opening to the tunnel that connects the α- and β-sites.

Comparison of the F9 and F19 complexes with E(Aex$_1$) to the corresponding E(Ain) complexes shows only minor differences at the α-site (Figure 5A,B). In the (F6)E(Aex$_1$) complex, only the orientation of αL2, which is important for intersubunit communication between the α- and β-subunits, was found to change. In comparison to the structure obtained at a relatively low F6 concentration [designated as the (low-F6)E(Ain) structure] (*23*) where αL2 is less defined in terms of the electron density of the side chains, the electron density is more visible in (F6)E(Aex$_1$), indicating a more ordered loop. A similar change was observed for the corresponding (high-F6)E(Ain) complex (*23*); this structure, obtained in the presence of high F6 concentrations, contained a second F6 molecule within the tunnel and also stabilized αL2. Compared to the (high-F6)E(Ain) complex, αL2 takes up the same conformation in (F6)E(Aex$_1$). The positions of the F6 ring and methylene groups in the α-active site are slightly different in all three F6 complexes, while the phosphoryl group and the carbonyl group positions are invariant, highlighting again the flexibility of the ligand (Figure 5C). While loop αL6 is not visible in any F6 complex, indicating an "open" state of the α-subunit, it takes up a partially closed conformation in the F9 and F19 complexes, as parts of the loop (residues α185−195) are still missing.

The structures of the β-subunit all have open conformations in the E(Aex$_1$) complexes presented herein. Panels D−F of Figure 5 compare details of the structures of the F9, F19, and F6 complexes with E(Ain) and E(Aex$_1$). The (F6)E(Aex$_1$) complex also exhibits the most significant change compared to the (low-F6)E(Ain) complex. The (low-F6)E(Ain) structure was shown previously to differ most from the F9 and F19 E(Ain) complexes. While binding of both F9 and F19 to E(Ain) is communicated via αL2 and βH6, the induced structuring and reorganization lead to an increased overall rigidity which orders the β-active site and primes it for L-Ser binding, whereas F6 binding in the (low-F6)E(Ain) structure lacks the ability to prime the enzyme to the same extent as the other ligands because the interdomain interface is more flexible and less ordered. The three ligand-bound E(Aex$_1$) structures are highly similar within experimental error [root-mean-square deviation (rmsd) values of 0.2 Å] compared to the (F9)E(Aex$_1$) complex. In these complexes, the structure of the β-site appears to be independent of the type of ligand bound to the α-site. The β-subunit of the (ASL)E(Aex$_1$) complex is, however, different from the so far observed ASL-bound internal aldimine states. The main differences reside within the COMM domain (residues β101−187), particularly in the region of residues β102−120 preceding and following loop βL3 (residues β110−115, which comprise the substrate carboxylate subsite), and in regions of residues β132−148 (residues impor-

tant for forming the closed conformation; see below) and β181−185 (residues that connect to one edge of the COMM domain). βH6 (residues β165−181) is the helix involved in the L-Ser- and ASL-mediated intersubunit communication between the α- and β-subunits. It is interesting to note that the conformation of this helix stays the same as that found in the internal aldimine structures (within experimental error). The overall change in the COMM domain in the (ASL)E-(Aex_1) complexes can be attributed to the formation of the external aldimine Schiff base group (PLS). The PLS group is tilted by 10° compared to the orientation of PLP in the internal aldimine structures. This rotation allows H-bonds between the PLS hydroxyl group and the carboxylate of βD305, and between the PLS carboxylate group and the main chain amides of βA112, βQ114, and βH115 (Figure 5D−F). These stabilizing contacts lead to a change in the β-subunit conformation by a main chain movement of β108−115 toward PLS which subsequently changes the positioning of β132−148 and β181−185. Since the neighboring regions are bound through tight intramolecular interactions, these residues are literally pulled along.

The (F6)E(Aex_1) complex displays additional differences, as the mobile state of the (low-F6)E(Ain) "catches up" structurally by adopting the "F9-/F19-like" external aldimine conformation directly. βH6 and residues β298−306 become as ordered as the same regions found in the (F9)E(Ain) and (F19)E(Ain) complexes. As a consequence of formation of PLS in the (F6)E(Aex_1) β-site, the carboxylate of βD305, which points away from PLP in the (F6)E(Ain) complex, swings in toward PLS to form the above-mentioned H-bond with the hydroxyl group of PLS (Figure 5F).

Crystal Structure of the (GP)E(A−A) Complex in the Presence of Cs and Low pH. The first crystal structure of the α-aminoacrylate intermediate that forms during stage I of the β-reaction (see Scheme 1) was determined at room temperature from a crystal mounted in a flow cell (*29*) with an L-Ser-containing buffer solution. The resulting structure shows the E(A−A) state with an open β-subunit conformation. In contrast to this structure, in the presence of GP, Cs^+, and low pH (pH 6.5), the E(A−A) complex was cryotrapped in a different conformation, displaying both α- and β-subdomains in closed conformations (Figure 6A).

The α-site is closed by αL6 which acts as a lid and which was completely visible in the electron density except for the three outermost residues (α190−192), which therefore were omitted from the model. GP is bound to the α-active site in the same way as in the βK87T mutant (*45*) with which the α-subdomain shares the highest degree of similarity (rmsd values in the range of 0.2−0.3 Å). The phosphoryl group is engaged in a H-bonding network with residues α234−236 of αH8′ and surrounding water molecules, while the 1-hydroxyl group H-bonds (2.7 Å) to the phenolic hydroxyl of αY175. αE49 takes up the inactive conformation, pointing away from the active site. Interestingly, this orientation differs slightly from the one observed in the (G3P)E(Ain) wild-type and (GP)$E^{\beta S178P}$(Ain) complexes (PDB entries 2CLK and 1K8Y, respectively). These changes reflect a minor overall change in the α-subunit (rmsd value of 0.2 for 1K8Y), including the regions that make up the active site. Due to these slight positional changes of αG184 and αG213 as well as αH8′, the ligand adopts a conformation that is unlike the one observed in all other GP- and G3P-complexed structures wherein the ligand always displays the same conformation when bound to the α-active site (Figure 6C).

The β-subunit of the Cs^+-stabilized (GP)E(A−A) complex at pH 6.5 exhibits a closed conformation previously observed only in βK87T E(Aex_1) mutant structures that were co-crystallized in the presence of both L-Ser and different α-site ligands (*45*). As a consequence of a rigid body movement of the COMM domain toward the C-terminal domain, both parts of the β-subunit are brought closer together, thus leading to a closure of the β-active site. In comparison with the (F−IPP)E(A−A)$_{open}$ complex (PDB entry 1A5S), the β-subunit shows large differences in some of the backbone positions (overall average rmsd value of 0.6 Å) (Figure 6A). The changes are especially large in the COMM domain (β122−185), the region of residues β285−310, and the C-terminal helix H13 (residues β375−394), with massive changes upon closure of the β-site giving rmsd values of 1.9 Å (β131−146), 1.5 Å (β154−178), and 1.2 Å (β284−306), respectively (Figure 6A). One particularly interesting aspect of the β-active site is the location of βE109 and water molecule 53. This water molecule makes contact with the β-C atom of the α-aminoacrylate moiety and is H-bonded to the carboxylate of βE109, a residue postulated to function as the acid−base catalytic group in β-replacement chemistry (Scheme 4) (*44*, *49*, *50*). This alignment is nearly correct for the βGlu109-assisted nucleophilic attack of WAT53 on the α-aminoacrylate to regenerate the L-Ser external aldimine (Figure 6D). Associated with these movements between the open and the closed β-active site are some changes in intramolecular contacts leading to a set of interactions consisting of a H-bonded salt bridge between βR141 and βD305 (*29*, *51*). It has been concluded from mutational studies that this salt bridge is crucial for the maintenance of the closed conformation (*17*, *18*). In the open conformation, βArg141 is usually solvent exposed while βD305 switches between so-called "flipped out" and "flipped in" conformations; in the latter, βD305 is involved in the coordination of the hydroxyl group of PLS in the E(Aex_1) open conformation state (*52*). Furthermore, in the closed, flipped out conformation, residues βQ142 and βR148 move significantly to form H-bonds to βK382 and βD383 and βQ114 and βG83, respectively.

Three Cs^+ ions were located in the structure, one of which occupies the monovalent cation binding site formed by the main chain carbonyl groups of βV231, βL232, βG268, βL304, and βF306. Although the radius of Cs^+ is larger than that of Na^+, the region is mainly unaltered compared to the (GP)E(Aex_1)$^{\beta K87T}$ complex in which the site is occupied by Na^+.

DISCUSSION

Allosteric Interactions Regulate Substrate Channeling in the Tryptophan Synthase Bienzyme Complex. Woehl and Dunn (*5*) demonstrated that the steady-state rate of substrate turnover in the β-reaction exhibits a primary KIE when [α-^{2}H]-L-Ser is substituted for isotopically normal L-Ser, establishing that the conversion of E(Aex_1) to E(A−A) is partially rate determining for turnover. In the overall αβ-reaction [reaction of IGP with L-Ser to give L-Trp (Scheme 1)], there is no isotope effect on the steady-state rate of

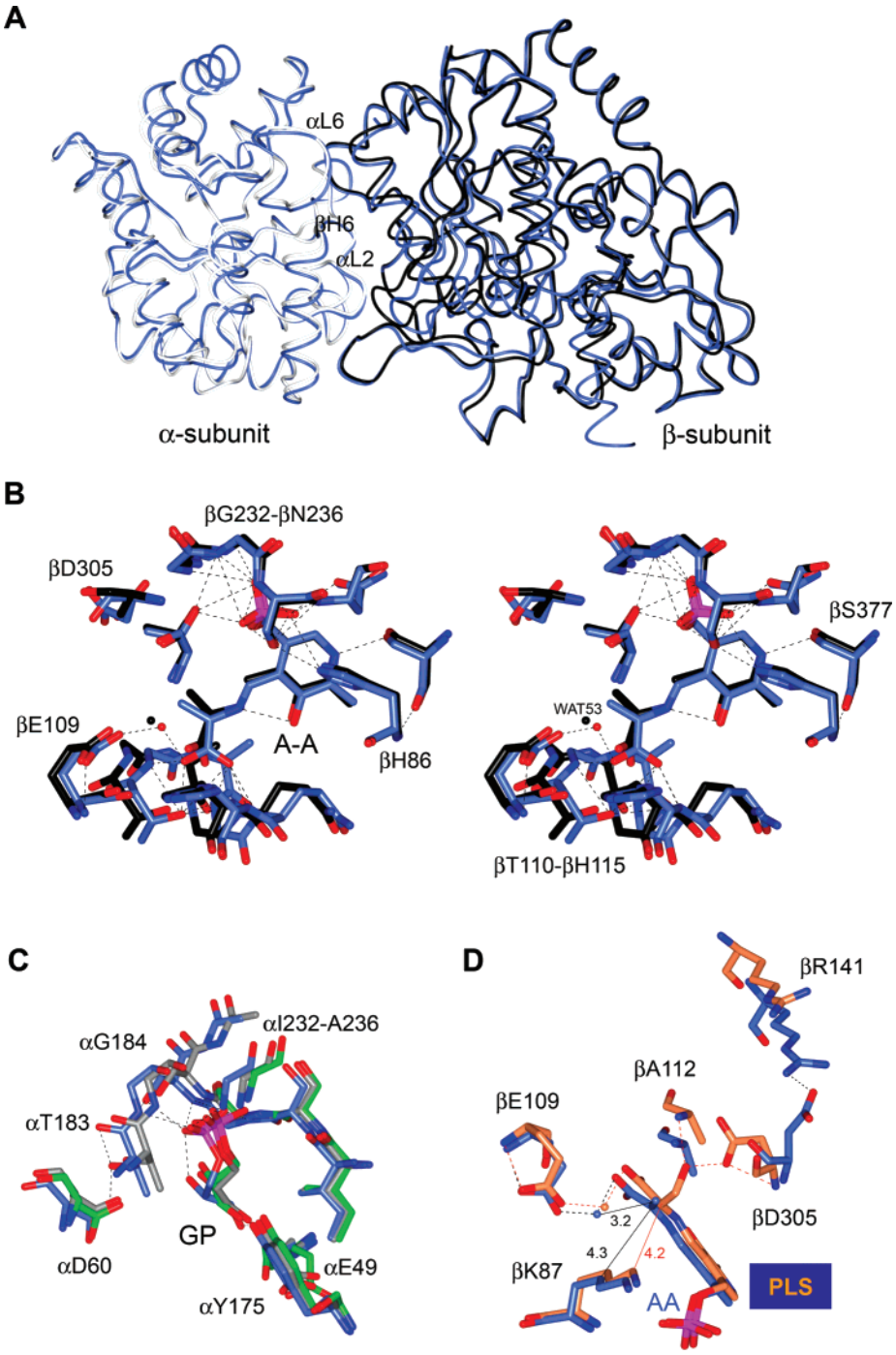

FIGURE 6: Structural features of the (GP)E(A−A) closed complex. (A) Superposition of the closed (GP)E(A−A) (light blue) and open (F-IPP)E(A−A) (white and black, PDB entry 1A5S) complexes. Both α- and *β*-subunits are shown and have been highlighted in contrasting colors for the (F-IPP)E(A−A) complex for better discrimination of the two subunits. (B) Stereoview of the structural details of the α-aminoacrylate bound to the *β*-active site in the open and closed E(A−A) complexes. The coloring is the same as in panel A. (C) Details of GP biding at the α-active site in different tryptophan synthase structures. The α-site of (GP)E(A−A) (light blue) was superpositioned with (GP)E(Ain) (gray, PDB entry 1WBJ) and (GP)E(Ain) for the *β*S178P mutant (green, PDB entry 1K8Y), and the interacting regions are displayed. (D) Details of the *β*-site of the open (F9)E(Aex_1) complex (coral) and the closed (GP)E(A−A) complex (light blue).

turnover, suggesting an event associated with reaction of IGP at the α-site becomes the rate-determining step (*6*). A considerable body of evidence has accumulated indicating that the regulation of substrate channeling in $\alpha_2\beta_2$ occurs through allosteric interactions consisting of ligand binding to the α-site, the binding and reaction of L-Ser at the *β*-site, and the binding of a monovalent cation (MVC) to the *β*-subunit at a site located close to the catalytic site (*1*, *8*−*11*, *13*, *28*, *45*). These allosteric interactions switch the two subunits between open (low-affinity, low-activity) and closed (high-affinity, high-activity) states, preventing the escape of the common metabolite, indole, and synchronizing the catalytic activities of the two sites so that the reactions are kinetically coupled (*1*, *3*, *4*, *7*, *8*, *14*). Formation of the E(A−A) intermediate at the *β*-site switches the α-site to the high-activity state (a >30-fold activation) (*3*, *8*, *9*). Conversion of E(Q_3) to E(Aex_2) switches the α-site back to the low-activity state (*3*, *4*) (Scheme 2).

Scheme 4: Proposed Acid−Base Catalytic Roles Played by βE109 in the β-Reaction

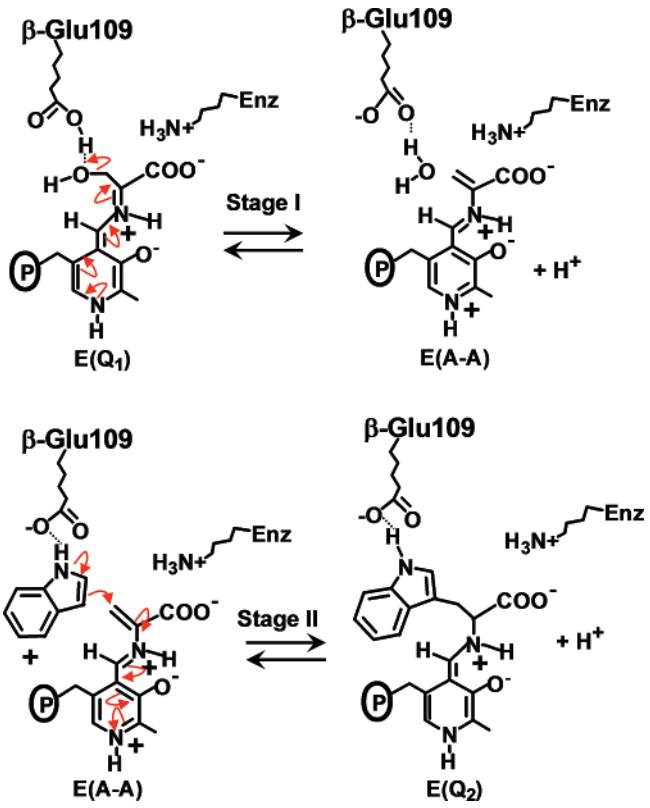

The binding of ASLs, such as IPP, GP, or G3P, increases the affinity of the β-site for ligands and alters the ground-state stabilities of intermediates formed in stage I of the β-reaction (*3*, *5*, *11*, *13*−*16*, *36*, *46*, *47*). The formation of the L-Trp quinonoid species in stage II of the β-reaction occurs ∼3-fold faster in the αβ-reaction than in the β-reaction (*3*, *6*), and this rate stimulation in the αβ-reaction appears to be due to the binding of G3P at the α-site. In this study, we demonstrate that the ASL activation of $1/\tau_2^{ASL}$ has the effect of activating stage I of the β-reaction.

Activation of the β-Reaction through Allosteric Interactions with the α-Site. The UV−vis absorption spectra presented in Figure 1 demonstrate that the binding of the new IGP analogues causes significant perturbations of the equilibrium distribution of intermediates formed in the reaction of L-Ser with E(Ain). Just as found for GP and G3P, the ASL-mediated redistribution increases the fraction of E(A−A) species at the expense of the $E(Aex_1)$ species. Among these analogues, F9 has the highest affinity for the enzyme (*23*) and F9 is the most effective at stabilizing E(A−A). Kinetic isotope effects (Figures 3 and 4) showed that the rate-determining step for the conversion of L-Ser to the α-aminoacrylate intermediate (stage I of the β-reaction) involves the abstraction of the C-α proton of the L-Ser external aldimine intermediate (*34*, *35*, *53*). The data presented in Figures 2−4 and Table 2 establish that binding of an ASL to the α-site can significantly activate this process. This activation involves an allosteric effect on the β-site that speeds the conversion of the $E(Aex_1)$ intermediate to E(A−A) by as much as 6−10-fold. The presence of a primary KIE establishes that this effect acts selectively on the conversion of $E(Aex_1)$ to E(A−A) (Figures 2−4 and Table 2). The data presented in Table 2 also show that ASL binding can slow the formation of $E(Aex_1)$. Depending on the structure of the ASL, the rate of $E(Aex_1)$ formation is slowed by 2−5-fold. Since the $1/\tau_1^{ASL} > 1/\tau_2^{ASL}$ relative order is retained for all ASLs listed in Table 2, the rate of E(A−A) formation remains limited by the magnitude of $1/\tau_2^{ASL}$. The result is a net overall enhancement of the rate of E(A−A) formation that is approximately equal to the enhancement of $1/\tau_2^{ASL}$. Hence, this allosteric interaction significantly activates a chemical step that occurs at a site on the β-subunit ∼25 Å away.

Here we consider two mechanistic explanations for the origins of this activation. The observation of a primary KIE on the decay phase when [α-^{2}H]-L-Ser is substituted for [α-^{1}H]-L-Ser requires that scission of the C−H bond at C-α of the $E(Aex_1)$ intermediate be a component of the rate-determining step (*5*, *34*, *35*, *53*). It is well-established that in the absence of ASLs the relaxation rate $1/\tau_2^{ASL}$ is dominated by the rate of conversion of $E(Aex_1)$ to $E(Q_1)$ (*5*, *35*). Since the apparent KIEs reported in Table 2 are different for the different ASLs, one explanation might be that ASL binding alters the extent to which C−H bond scission occurs in the transition state. We consider this explanation unlikely because it would imply a different β-site conformation for each ASL complex in the transition state.

We think it is much more likely that the variation of the apparent isotope effect with ASL structure is due to the fact that $1/\tau_2^{ASL}$ is a kinetically complicated parameter; i.e., C−H bond scission is only partially rate determining. Because C−H bond cleavage is not the only process contributing to $1/\tau_2^{ASL}$, the observed KIEs are not the intrinsic isotope effects for bond scission (*5*). Thus, $1/\tau_2^{ASL}$ also may have rate contributions from the preceding chemical steps in catalysis and from the interconversion of protein conformation states (viz., Scheme 1 and eq 2). The differences in the values of $1/\tau_1^{ASL}$ and $1/\tau_2^{ASL}$ are not so large that they are kinetically well separated for each of the ASLs (*54*). Thus, rate constants from the preceding chemical step(s) contribute to $1/\tau_2^{ASL}$, and the extent of this contribution differs for each ASL. Of similar importance, earlier studies (*5*, *6*) indicated that $E(Aex_1)$ rapidly interconverts between open and closed conformations at rates that are rapid with respect to $1/\tau_1^{ASL}$ and $1/\tau_2^{ASL}$. If, as it appears (*5*), one conformation (closed) is significantly more reactive than the other (open), then the distribution between open and closed states also will influence the values of both $1/\tau_2^{ASL}$ and the apparent KIE.

Structural Origins of Catalysis in Stage I of the β-Reaction. Previous structural studies of the reaction intermediates in the β-reaction have yielded almost exclusively complexes with the β-subunits in the open conformation (*16*). These structures include three external aldimines (1BEU, 1KFE, and 1KFJ) (*52*, *55*) and the α-aminoacrylate (1A5S) (*29*), all resulting from the reaction of L-Ser. Structures with the β-subunits in the closed conformation have proven to be much more difficult to generate. Rhee et al. (*45*) published the structures of four complexes in which the active site Lys residue (βK87) was replaced with Thr. Three of these mutant complexes gave β-subunits with closed conformations [two L-Ser external aldimine structures (2TSY and 2TRS) and one L-Trp external aldimine structure (2TYS)], and the fourth mutant structure (1UBS) gave an open β-subunit conformation of the L-Ser external aldimine.

The structures of external aldimine and α-aminoacrylate complexes presented in this report provide new information about the catalytic mechanism and allosteric regulation of stage I of the β-reaction. On the basis of this new information, we present the following mechanistic hypothesis for catalysis in stage I. We propose that the open conformation of the β-subunits of the (F9)E(Aex_1) complex corresponds to a low-activity form of the enzyme similar to earlier external aldimine structures (*52*) that appear to be stabilized by low temperatures and crystal lattice forces. Conversely, the β-subunit of the Cs^+ form of the (GP)E(A−A) complex presents a closed form we propose corresponds to an activated β-site stabilized by the lower pH (pH 6.5) and by the stronger allosteric effects exerted by Cs^+ versus Na^+ (*28*, *36*, *37*, *40*, *41*).

The arguments for this interpretation of the new structural information are as follows. The complex formed with F9 and L-Ser shows an external aldimine structure, (F9)E(Aex_1), for the PLS moiety, although (F9)E(A−A) is significantly more stable at pH 7.8 and room temperature in solution (*23*). The β-subunit of the (F9)E(Aex_1) complex exhibits clear structural signatures of the open conformation, including the absence of the βD305−βR141 salt bridge and the COMM domain very similar to the open β-subunit conformations found in most published structures (*23*, *29*, *44*, *46*−*48*, *51*, *52*, *55*, *56*). The (F9)E(Aex_1) structure is also characterized by a H-bonding interaction between the PLS hydroxyl and the side chain of βD305 that is similar to the open external aldimine structures reported by Kulik et al. (*52*). There is no reason to expect that the βD305 side chain is protonated in these structures under the given experimental conditions. Consequently, the H-bond to the carboxylate will function chemically to help stabilize the E(Aex_1) structure relative to E(A−A) and make elimination more difficult. With βD305 tied up in this H-bonding interaction, the salt bridge between βR141 and βD305 cannot be formed and the closed conformation of the β-subunit is rendered unstable. While βD305 is important for substrate specificity and allosteric communication (*16*−*18*, *29*), it seems unlikely that this residue functions as the acid−base catalyst in the β-elimination and β-addition steps. Solution studies have provided strong evidence supporting βE109 as the acid−base catalyst in the elimination step (*20*, *45*, *50*), and the structure of the (GP)E(A−A) complex shows this residue is ideally located to play this role (Figure 6B and Scheme 4). Indeed, comparison of the (F9)E(Aex_1) and (GP)E(A−A) structures provides strong evidence that the primary function of βD305 is as a switch in the transmission of allosteric effects between the β- and α-sites (see below).

In contrast to the (F9)E(Aex_1) complex, the (GP)E(A−A) complex is the first example of a tryptophan synthase structure in which the native form of the enzyme exhibits a closed conformation. Rhee et al. (*45*) were the first to report closed structures of the β-subunit; however, these structures all involve mutant enzyme species with the essential active site lysine residue, βK87, replaced with Thr. The resulting catalytically inactive enzyme was found to give external aldimine complexes with closed conformations of the β-subunit. However, because of the lack of catalytic activity and structural perturbations resulting from the βK87T mutation, the mechanistic significance of these structures was unclear. Inferences from solution studies dating back to 1990 (*1*, *3*−*10*, *13*−*16*, *21*, *22*, *28*, *38*, *40*−*42*, *52*, *57*) have provided clear evidence that the switching between open and closed conformations of the α- and β-subunits is essential for catalysis and allosteric regulation of substrate channeling in tryptophan synthase. The closed structure of the (GP)E(A−A) complex presented herein provides new information essential for the understanding of catalysis and allosteric regulation. Examination of the β-subunit structure shows that βR141 forms a H-bonded salt bridge with one oxygen of the carboxylate (OD2) of βD305. In this conformation, the side chain of βD305 is rotated to a position ∼10 Å from the β-carbon of the α-aminoacrylate external aldimine. However, βE109 is located 5.8 Å from the α-aminoacrylate C-β and is H-bonded (2.8 Å) to an intervening water molecule (WAT53) that is close to C-β (3.2 Å) of the α-aminoacrylate group (Figure 6B). If we allow for minor motions in the side chain, the position of βE109 appears to be appropriate either for catalysis of the nucleophilic attack of a water [conversion back to E(Q_1)] (Scheme 4) or, following the binding of indole, for catalysis in stage II of the attack of indole on the double bond via stabilization of the developing positive charge on the indole ring nitrogen [conversion to E(Q_2)] (Figure 6B and Scheme 4). Consequently, the (GP)E(A−A) structure strongly supports a mechanism for the β-reaction in which βE109 plays a critically important acid−base role in catalysis of the β-replacement chemistry (*20*, *44*, *45*, *50*) via the closed β-subunit conformation (viz. Scheme 4).

As depicted in Figure 6D and Scheme 4, βE109 is proposed to play the role of acid−base catalyst in the interactions at the β-site that catalyze the interconversion of E(Q_1) and E(A−A). The structures in Figure 6D show that the hydroxyl of PLS starts out in an inactive conformation with H-bonds to the NH group of βA112 and to the carboxylate of βD305 in the (F9)E(Aex_1) complex and, presumably, ends up as a water molecule at the position occupied by WAT53 in the (GP)E(A−A) complex. As E(Aex_1) is converted to E(Q_1) and then to E(A−A), this hydroxyl must rotate to a location that overlaps the positions of WAT60 and WAT53 in these structures to receive a proton from the carboxylic acid group of βE109 via a new H-bonding interaction. This repositioning of the PLS hydroxyl appears to be driven by the conversion of the open E(Aex_1) conformation to the corresponding closed conformation. This conformational change causes a displacement of the COMM domain which results in the movement of βR141 and βD305 closer together by ∼1.3 Å, movement of βA112 away from PLS by ∼0.8 Å, the flipping of the βD305 carboxylate by ∼100°, and formation of the βR141−βAsp305 salt bridge. These motions remove the stabilizing interactions of the PLS hydroxyl with βD305 and βA112, allowing it to rotate by 120−130° to the WAT60/WAT53 position to H-bond with βE109. This rearrangement of site and substrate groups positions the PLS hydroxyl for the proton transfer needed during the elimination step. Elimination then occurs via abstraction of the E(Aex_1) C-α proton by βK87 to form E(Q_1) followed by proton transfer from βE109 to the hydroxyl oxygen as C−O bond scission takes place.

Regulation of β-Site Catalysis by ASL Binding. We hypothesize that catalysis in the β-reaction proceeds via closed structures at each step of the reaction. However, in

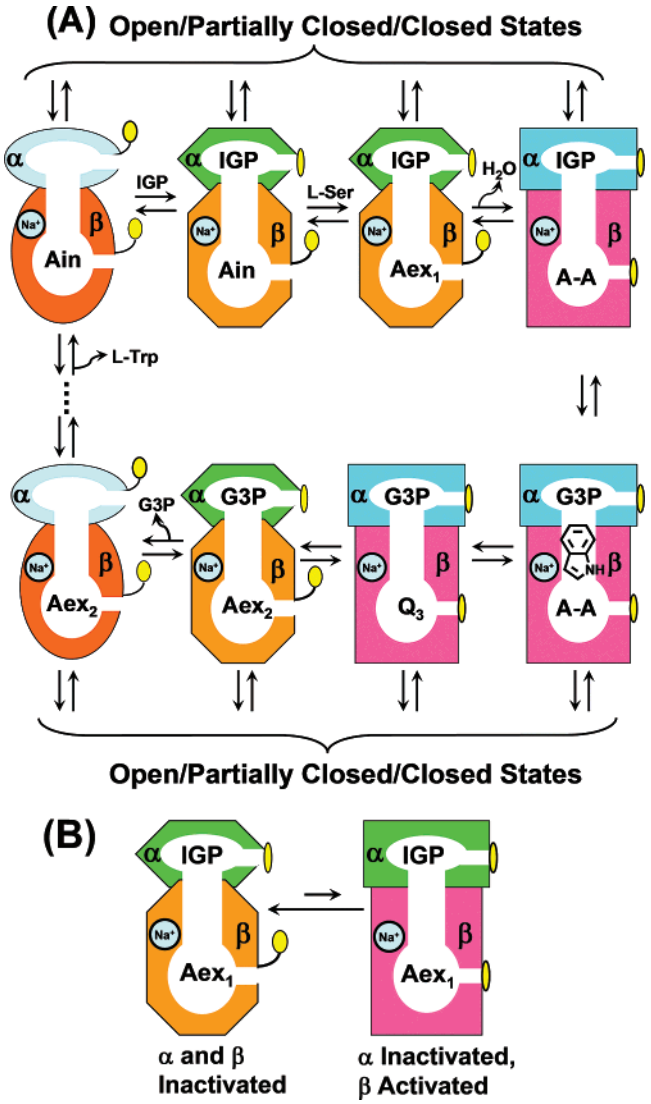

FIGURE 7: Cartoon summarizing the proposed relationship between conformation states[2] and activity states for an αβ-dimeric unit of the tetrameric enzyme during the αβ-reaction. (A) Cartoon depicting the predominating conformational states of αβ-dimeric units in the αβ-reaction cycle: rectangles for closed and ellipses, hexagons, and octagons for open/partially closed. Blue (α) and magenta (β) subunits are activated. Lids are colored yellow. Vertical arrows above and below the diagram indicate the presence of conformational equilibria linked to additional open and partially closed/closed states. (B) Interconversion of the inactive and activated (IGP)E-(Aex_1) complexes.

stage I of the β-reaction, conformational equilibria favor the open/partially closed, less reactive states in solution for E(Ain), E(GD_1), and E(Aex_1), while E(Q_1) and E(A−A) are predominantly in the closed conformation (*1*, *57*). According to this hypothesis, both the slowing of external aldimine formation and the activation of conversion of E(Aex_1) to E(A−A) would occur by shifting the distribution of conformations toward the closed (active) state. If binding/dissociation occurs via the open/partially closed conformations, then a shift in the distribution toward the closed state could have the effect of slowing the observed rate of complex formation and hence the rate of E(Aex_1) formation. An increase in the rate of E(A−A) formation could occur as follows. As an example, suppose in the absence of an ASL, one of every 100 molecules of E(Aex_1) was in the active conformation (K = [active]/[inactive] = 1/99 = 0.01) and ASL binding changed this distribution to nine of every 100 molecules (K^{ASL} = 9/91 = 0.099). Then, provided that the interconversion between open and closed states is rapid in comparison to the chemical transformations, the binding of the ASL would bring about an ~10-fold activation (K^{ASL}/K = 0.099/0.0101 = 9.8). According to this scenario, the inactive conformation would still predominate even when the ASL is bound. This mechanism also requires that during the steps involved in the conversion of E(Ain) to E(Q_1), the switching between open/partially closed and closed conformations of the β-site is relatively rapid, allowing for the relatively rapid formation of E(Aex_1) and for a rate-limiting abstraction of the C-α proton of E(Aex_1) as E(Aex_1) is converted to E(A−A) via E(Q_1).

Regulation of Substrate Channeling and Activation of Stage I of the β-Reaction. The solution studies and crystal structures presented in this work and in the studies of ref *23* indicate the new artificial ASLs under investigation mimic the allosteric properties of G3P, GP, IPP, and indole-3-acetylglycine (IAG) (*1*, *3*, *8*, *13*, *34*, *46*, *47*, *58*). Therefore, in the following discussion of mechanism, we postulate that IGP binding elicits allosteric interactions similar to those revealed by the artificial ASLs and by G3P. On the basis of this premise, the new insights derived from these ASLs and from G3P are incorporated into the regulatory mechanism (Figure 7) as follows.

(1) IGP binding, like the binding of other ASLs, switches the α-site to a closed/partially closed conformation[2] which facilitates changes in the β-subunit that give rise to an increase in the affinity of the β-site for L-Ser (*23*, *24*).

(2) By analogy to the allosteric properties of the ASLs, IGP binding activates stage I of the β-reaction through allosteric interactions. These allosteric interactions function to activate the rate-determining step for E(A−A) formation, a process which includes scission of the Cα−H σ-bond of E(Aex_1) (Scheme 1A). The analogue studies show this rate enhancement of stage I could be as much as 8−10-fold in the physiological αβ-reaction (Figures 2−4 and Table 2). Because Cα−H bond scission is not rate-determining in the αβ-reaction, the magnitude of this rate enhancement has not been established for IGP. The experiments of Woehl et al. (*6*) and Brzovic et al. (*3*) indicate an enhancement of at least 3-fold.

(3) Formation of E(A−A), in turn, triggers an allosteric conformational change in the α-subunit that closes the α-active site completely, thereby increasing the affinity of

[2] The structures of various tryptophan synthase complexes suggest that the α-subunit may interconvert among three conformational states, open, partially closed, and closed. The absence of substrates or substrate analogues gives the conformation where both the α- and β-sites reside in the open conformation, and in the crystalline state, αL6 is completely disordered. In the structures where the β-domain is closed and the α-site is occupied by an ASL, the electron densities for loop αL6 (residues α179−192) are well-defined (with the exception of the two outermost residues in some structures). On the basis of this crystallographic evidence, these structures clearly exhibit closed α- and β-subunits. In structures where the β-subunit is not closed and the α-site is occupied, only parts of αL6 are visible in the electron density maps (residues α179−183 in most cases). These structures may represent a partially closed state. Since we do not understand how crystal lattice packing forces influence the conformation and mobility of αL6, it is not clear that the disorder observed in these structures corresponds to well-defined conformation states in solution.

the α-site for IGP (and IGP analogues) and activating cleavage of IGP by >30-fold (Scheme 2) (*1*, *3*, *4*, *7*−*9*, *52*). At this point in the α*β*-reaction cycle, the α*β*-dimeric units of the tetrameric $\alpha_2\beta_2$ complex have switched to the closed conformation and the α- and *β*-sites are both activated.

(4) Following cleavage of IGP, indole diffuses along the tunnel into the *β*-site and reacts with E(A−A) to form $E(Q_2)$, which is quickly transformed to $E(Q_3)$. Then, $E(Q_3)$ is converted to the tryptophan external aldimine, $E(Aex_2)$ (*12*, *34*).

(5) The α-site remains in the closed conformation with G3P (*23*) bound during the portion of the *β*-catalytic cycle where the E(A−A), $E(Q_2)$, and $E(Q_3)$ intermediates form and decay (*1*, *3*, *4*).

(6) Conversion of $E(Q_3)$ to $E(Aex_2)$ switches the α-site back to a distribution strongly favoring the open, low-affinity, low-activity state (*1*, *3*).

(7) G3P remains bound to the α-site until $E(Aex_2)$ formation occurs, and then G3P dissociates from the α-site when the *β*-site switches to the open conformation (*1*).

(8) $E(Aex_2)$ is converted via $E(GD_2)$ to E(Ain) and L-Trp, and the *β*-site is switched to the predominating open, low-activity state (*1*, *3*).

(9) The *β*-site remains primarily in the low-activity state until IGP binds in the subsequent catalytic cycle. The α-site remains in the low-activity state until the *β*-site again is converted to the E(A−A) species (Scheme 2) (*1*). This interdependence of conformational states on binding and covalent reaction events at the two sites functions to synchronize the activities of the α- and *β*-sites.

In conclusion, this work establishes that ASL structural mimics of IGP or G3P activate stage I of the *β*-reaction, a finding that provides strong indirect evidence that IGP behaves similarly. When taken together with the discovery that E(A−A) formation is the covalent process which activates the α-site (*1*, *3*, *4*, *8*), it is now clear that the channeling of indole is modulated by a very intricate set of reciprocal allosteric interactions that control and synchronize the catalytic activities, substrate affinities, and site accessibilities of the bienzyme complex.

ACKNOWLEDGMENT

I.S. thanks the beamline staff at the ESRF and SLS for help setting up the experiments.

REFERENCES

1. Pan, P., Woehl, E., and Dunn, M. F. (1997) Protein architecture, dynamics and allostery in tryptophan synthase channeling, *Trends Biochem. Sci. 22*, 22−27.
2. Miles, E. W., Rhee, S., and Davies, D. R. (1999) The molecular basis of substrate channeling, *J. Biol. Chem. 274*, 12193−12196.
3. Brzovic, P. S., Ngo, K., and Dunn, M. F. (1992) Allosteric interactions coordinate catalytic activity between successive metabolic enzymes in the tryptophan synthase bienzyme complex, *Biochemistry 31*, 3831−3839.
4. Leja, C. A., Woehl, E. U., and Dunn, M. F. (1995) Allosteric linkages between *β*-site covalent transformations and α-site activation and deactivation in the tryptophan synthase bienzyme complex, *Biochemistry 34*, 6552−6561.
5. Woehl, E., and Dunn, M. F. (1999) Mechanisms of monovalent cation action in enzyme catalysis: The first stage of the tryptophan synthase *β*-reaction, *Biochemistry 38*, 7118−7130.
6. Woehl, E., and Dunn, M. F. (1999) Mechanisms of monovalent cation action in enzyme catalysis: The tryptophan synthase α-, *β*-, and α*β*-reactions, *Biochemistry 38*, 7131−7141.
7. Kirschner, K., Lane, A. N., and Strasser, A. W. M. (1991) Reciprocal communication between the lyase and synthase active-sites of the tryptophan synthase bienzyme complex, *Biochemistry 30*, 472−478.
8. Anderson, K. S., Miles, E. W., and Johnson, K. A. (1991) Serine modulates substrate channeling in tryptophan synthase: A novel intersubunit triggering mechanism, *J. Biol. Chem. 266*, 8020−8033.
9. Kawasaki, H., Bauerle, R., Zon, G., Ahmed, S. A., and Miles, E. W. (1987) Site-specific mutagenesis of the α subunit of tryptophan synthase from *Salmonella typhimurium*. Changing arginine 179 to leucine alters the reciprocal transmission of substrate-induced conformational changes between the α and β_2 subunits, *J. Biol. Chem. 262*, 10678−10683.
10. Houben, K. F., Kadima, W., Roy, M., and Dunn, M. F. (1989) L-Serine analogues form Schiff base and quinonoidal intermediates with *Escherichia coli* tryptophan synthase, *Biochemistry 28*, 4140−4147.
11. Houben, K. F., and Dunn, M. F. (1990) Allosteric effects acting over a distance of 20−25 Å in the *Escherichia coli* tryptophan synthase bienzyme complex increase ligand affinity and cause redistribution of covalent intermediates, *Biochemistry 29*, 2421−2429.
12. Drewe, W. F., Jr., and Dunn, M. F. (1986) Characterization of the reaction of L-serine and indole with *Escherichia coli* tryptophan synthase via rapid-scanning ultraviolet-visible spectroscopy, *Biochemistry 25*, 2494−2501.
13. Dunn, M. F., Aguilar, V., Brzovic, P., Drewe, W. F., Jr., Houben, K. F., Leja, C. A., and Roy, M. (1990) The tryptophan synthase bienzyme complex transfers indole between the α- and *β*-sites via a 25−30 Å long tunnel, *Biochemistry 29*, 8598−8607.
14. Brzovic, P. S., Sawa, Y., Hyde, C. C., Miles, E. W., and Dunn, M. F. (1992) Evidence that mutations in a loop region of the α-subunit inhibit the transition from an open to a closed conformation in the tryptophan synthase bienzyme complex, *J. Biol. Chem. 267*, 13028−13038.
15. Brzovic, P. S., Hyde, C. C., Miles, E. W., and Dunn, M. F. (1993) Characterization of the functional role of a flexible loop in the α-subunit of tryptophan synthase from *Salmonella typhimurium* by rapid-scanning, stopped-flow spectroscopy and site-directed mutagenesis, *Biochemistry 32*, 10404−10413.
16. Weber-Ban, E., Hur, O., Bagwell, C., Banik, U., Yang, L. H., Miles, E. W., and Dunn, M. F. (2001) Investigation of allosteric linkages in the regulation of tryptophan synthase: The roles of salt bridges and monovalent cations probed by site-directed mutation, optical spectroscopy, and kinetics, *Biochemistry 40*, 3497−3511.
17. Ferrari, D., Yang, L. H., Miles, E. W., and Dunn, M. F. (2001) *β*D305A mutant of tryptophan synthase shows strongly perturbed allosteric regulation and substrate specificity, *Biochemistry 40*, 7421−7432.
18. Ferrari, D., Niks, D., Yang, L. H., Miles, E. W., and Dunn, M. F. (2003) Allosteric communication in the tryptophan synthase bienzyme complex: Roles of the *β*-subunit aspartate 305-arginine 141 salt bridge, *Biochemistry 42*, 7807−7818.
19. Marabotti, A., Cozzini, P., and Mozzarelli, A. (2000) Novel allosteric effectors of the tryptophan synthase $\alpha_2\beta_2$ complex identified by computer-assisted molecular modeling, *Biochim. Biophys. Acta 1476*, 287−299.
20. Osborne, A., Teng, Q., Miles, E. W., and Phillips, R. S. (2003) Detection of open and closed conformations of tryptophan synthase by ^{15}N-heteronuclear single-quantum coherence nuclear magnetic resonance of bound 1-^{15}N-L-tryptophan, *J. Biol. Chem. 278*, 44083−44090.
21. Harris, R. M., and Dunn, M. F. (2002) Intermediate trapping via a conformational switch in the Na^+-activated tryptophan synthase bienzyme complex, *Biochemistry 41*, 9982−9990.
22. Harris, R. M., Ngo, H., and Dunn, M. F. (2005) Synergistic effects on escape of a ligand from the closed tryptophan synthase bienzyme complex, *Biochemistry 44*, 16886−16895.
23. Ngo, H., Harris, R., Kimmich, N., Casino, P., Niks, D., Blumenstein, L., Barends, T. R., Kulik, V., Weyand, M., Schlichting, I., and Dunn, M. F. (2007) Synthesis and characterization of allosteric probes of substrate channeling in the tryptophan synthase bienzyme complex, *Biochemistry 46*, 7713−7727.
24. Casino, P., Niks, D., Ngo, H., Pan, P., Brzovic, P., Kulik, V., Schlichting, I., and Dunn, M. F. (2007) Allosteric regulation of

tryptophan synthase channeling: The internal aldimine probed by *trans*-3-indole-3′-acrylate binding, *Biochemistry 46*, 7728−7739.
25. Miles, E. W. (1995) Tryptophan synthase. Structure, function, and protein engineering, *Subcell. Biochem. 24*, 207−254.
26. Miles, E. W., Bauerle, R., and Ahmed, S. A. (1987) Tryptophan synthase from *Escherichia coli* and *Salmonella typhimurium*, *Methods Enzymol. 142*, 398−414.
27. Yang, L., Ahmed, S. A., and Miles, E. W. (1996) PCR mutagenesis and overexpression of tryptophan synthase from *Salmonella typhimurium*: On the roles of β_2 subunit Lys-382, *Protein Expression Purif. 8*, 126−136.
28. Woehl, E. U., and Dunn, M. F. (1995) Monovalent metal ions play an essential role in catalysis and intersubunit communication in the tryptophan synthase bienzyme complex, *Biochemistry 34*, 9466−9476.
29. Schneider, T. R., Gerhardt, E., Lee, M., Liang, P. H., Anderson, K. S., and Schlichting, I. (1998) Loop closure and intersubunit communication in tryptophan synthase, *Biochemistry 37*, 5394−5406.
30. Kabsch, W. (1993) Automatic processing of rotation diffraction data from crystals of initially unknown symmetry and cell constants, *J. Appl. Crystallogr. 26*, 795−800.
31. Brunger, A. T., Adams, P. D., Clore, G. M., Delano, W. L., Gros, P., Grosse-Kunstleve, R. W., Jiang, J. S., Kuszewski, J., Nilges, M., Pannu, N. S., Read, R. J., Rice, L. M., Simonson, T., and Warren, G. L. (1998) Crystallography & NMR system: A new software suite for macromolecular structure determination, *Acta Crystallogr. D54*, 905−921.
32. Jones, T. A., Zou, J. Y., Cowan, S. W., and Kjeldgaard, M. (1991) Improved methods for building protein models in electron-density maps and the location of errors in these models, *Acta Crystallogr. A47*, 110−119.
33. McRee, D. E. (1999) XtalView Xfit: A versatile program for manipulating atomic coordinates and electron density, *J. Struct. Biol. 125*, 156−165.
34. Lane, A. N., and Kirschner, K. (1983) The mechanism of binding of L-serine to tryptophan synthase from *Escherichia coli*, *Eur. J. Biochem. 129*, 561−570.
35. Drewe, W. F., Jr., and Dunn, M. F. (1985) Detection and identification of intermediates in the reaction of L-serine with *Escherichia coli* tryptophan synthase via rapid-scanning ultraviolet-visible spectroscopy, *Biochemistry 24*, 3977−3987.
36. Fan, Y. X., McPhie, P., and Miles, E. W. (2000) Regulation of tryptophan synthase by temperature, monovalent cations, and an allosteric ligand. Evidence from Arrhenius plots, absorption spectra, and primary kinetic isotope effects, *Biochemistry 39*, 4692−4703.
37. Hur, O., Niks, D., Casino, P., and Dunn, M. F. (2002) Proton transfers in the β-reaction catalyzed by tryptophan synthase, *Biochemistry 41*, 9991−10001.
38. Phillips, R. S., Miles, E. W., Holtermann, G., and Goody, R. S. (2005) Hydrostatic pressure affects the conformational equilibrium of *Salmonella typhimurium* tryptophan synthase, *Biochemistry 44*, 7921−7928.
39. Miles, E. W. (1979) Tryptophan synthase: Structure, function, and subunit interaction, *Adv. Enzymol. Relat. Areas Mol. Biol. 49*, 127−186.
40. Peracchi, A., Mozzarelli, A., and Rossi, G. L. (1995) Monovalent cations affect dynamic and functional properties of the tryptophan synthase $\alpha_2\beta_2$ complex, *Biochemistry 34*, 9459−9465.
41. Peracchi, A., Bettati, S., Mozzarelli, A., Rossi, G. L., Miles, E. W., and Dunn, M. F. (1996) Allosteric regulation of tryptophan synthase: Effects of pH, temperature, and α-subunit ligands on the equilibrium distribution of pyridoxal 5′-phosphate-L-serine intermediates, *Biochemistry 35*, 1872−1880.
42. Fan, Y. X., McPhie, P., and Miles, E. W. (1999) Guanidine hydrochloride exerts dual effects on the tryptophan synthase alpha $\alpha_2\beta_2$ complex as a cation activator and as a modulator of the active site conformation, *Biochemistry 38*, 7881−7890.
43. Lane, A. N., and Kirschner, K. (1981) The mechanism of tryptophan binding to tryptophan synthase from *Escherichia coli*, *Eur. J. Biochem. 120*, 379−387.
44. Hyde, C. C., Ahmed, S. A., Padlan, E. A., Miles, E. W., and Davies, D. R. (1988) Three-dimensional structure of the tryptophan synthase $\alpha_2\beta_2$ multienzyme complex from *Salmonella typhimurium*, *J. Biol. Chem. 263*, 17857−17871.
45. Rhee, S., Parris, K. D., Hyde, C. C., Ahmed, S. A., Miles, E. W., and Davies, D. R. (1997) Crystal structures of a mutant (βK87T) tryptophan synthase $\alpha_2\beta_2$ complex with ligands bound to the active sites of the α- and β-subunits reveal ligand-induced conformational changes, *Biochemistry 36*, 7664−7680.
46. Weyand, M., Schlichting, I., Marabotti, A., and Mozzarelli, A. (2002) Crystal structures of a new class of allosteric effectors complexed to tryptophan synthase, *J. Biol. Chem. 277*, 10647−10652.
47. Weyand, M., Schlichting, I., Herde, P., Marabotti, A., and Mozzarelli, A. (2002) Crystal structure of the βSer178 → Pro mutant of tryptophan synthase. A "knock-out" allosteric enzyme, *J. Biol. Chem. 277*, 10653−10660.
48. Kulik, V., Hartmann, E., Weyand, M., Frey, M., Gierl, A., Niks, D., Dunn, M. F., and Schlichting, I. (2005) On the structural basis of the catalytic mechanism and the regulation of the α subunit of tryptophan synthase from *Salmonella typhimurium* and BX1 from maize, two evolutionarily related enzymes, *J. Mol. Biol. 352*, 608−620.
49. Miles, E. W. (1991) Structural Basis for Catalysis by Tryptophan Synthase, *Adv. Enzymol. Relat. Areas Mol. Biol. 64*, 93.
50. Brzovic, P. S., Kayastha, A. M., Miles, E. W., and Dunn, M. F. (1992) Substitution of glutamic acid 109 by aspartic acid alters the substrate specificity and catalytic activity of the β-subunit in the tryptophan synthase bienzyme complex from *Salmonella typhimurium*, *Biochemistry 31*, 1180−1190.
51. Rhee, S., Miles, E. W., and Davies, D. R. (1998) Cryocrystallography of a true substrate, indole-3-glycerol phosphate, bound to a mutant (αD60N) tryptophan synthase $\alpha_2\beta_2$ complex reveals the correct orientation of active site αGlu49, *J. Biol. Chem. 273*, 8553−8555.
52. Kulik, V., Weyand, M., Seidel, R., Niks, D., Arac, D., Dunn, M. F., and Schlichting, I. (2002) On the role of αThr183 in the allosteric regulation and catalytic mechanism of tryptophan synthase, *J. Mol. Biol. 324*, 677−690.
53. Miles, E. W., and McPhie, P. (1974) Evidence for a rate-determining proton abstraction in the serine deaminase reaction of the β_2 subunit of tryptophan synthetase, *J. Biol. Chem. 249*, 2852−2857.
54. Bernasconi, C. (1976) *Relaxation Kinetics*, Academic Press, New York.
55. Rhee, S., Miles, E. W., Mozzarelli, A., and Davies, D. R. (1998) Cryocrystallography and microspectrophotometry of a mutant (αD60N) tryptophan synthase $\alpha_2\beta_2$ complex reveals allosteric roles of αAsp60, *Biochemistry 37*, 10653−10659.
56. Rhee, S., Parris, K. D., Ahmed, S. A., Miles, E. W., and Davies, D. R. (1996) Exchange of K^+ or Cs^+ for Na^+ induces local and long-range changes in the three-dimensional structure of the tryptophan synthase $\alpha_2\beta_2$ complex, *Biochemistry 35*, 4211−4221.
57. Pan, P., and Dunn, M. F. (1996) β-Site covalent reactions trigger transitions between open and closed conformations of the tryptophan synthase bienzyme complex, *Biochemistry 35*, 5002−5013.
58. Marabotti, A., De Biase, D., Tramonti, A., Bettati, S., and Mozzarelli, A. (2001) Allosteric communication of tryptophan synthase. Functional and regulatory properties of the βS178P mutant, *J. Biol. Chem. 276*, 17747−17753.
59. Yanofsky, C., and Crawford, I. P. (1972) Tryptophan Synthase, in *The Enzyme* (Boyer, P. D., Ed.) 3rd ed., pp 1−31, Academic Press, New York.

BI7003872